Title

In Situ Liquid Cell Observations of Asbestos Fiber Diffusion in Water

Journal

Environmental Science and Technology, 49(22)

ISSN

0013-936X

Authors

Wu, Lei
Ortiz, Carlos
Xu, Ye
et al.

Publication Date

2015-11-17

DOI

10.1021/acs.est.5b03839

Peer reviewed

Environmental Science & Technology

Article

pubs.acs.org/est

In Situ Liquid Cell Observations of Asbestos Fiber Diffusion in Water

Lei Wu,[†] Carlos Ortiz,[†,‡] Ye Xu,[‡] Jane Willenbring,[†] and Douglas Jerolmack*[,†]

[†]Department of Earth and Environmental Science, and [‡]Department of Physics and Astronomy, University of Pennsylvania, Philadelphia, Pennsylvania 19104, United States

Supporting Information

ABSTRACT: We present real-time observations of the diffusion of individual asbestos fibers in water. We first scaled up a technique for fluorescent tagging and imaging of chrysotile asbestos fibers and prepared samples with a distribution of fiber lengths ranging from 1 to 20 μm. Experiments were then conducted by placing a 20, 100, or 150 ppm solution of these fibers in a liquid cell mounted on a spinning-disk confocal microscope. Using automated elliptical-particle detection methods, we determined the translation and rotation and two-dimensional (2D) trajectories of thousands of diffusing chrysotile fibers. We find that fiber diffusion is size-dependent and in reasonable agreement with theoretical predictions for the Brownian motion of rods. This agreement is remarkable given that experiments involved non-idealized particles at environmentally relevant concentrations in a confined cell, in which particle−particle and particle−wall interactions might be expected to cause deviations from theory. Experiments also confirmed that highly elongated chrysotile fibers exhibit anisotropic diffusion at short time scales, a predicted effect that may have consequences for aggregate formation and transport of asbestos in confined spaces. The examined fibers vary greatly in their lengths and were prepared from natural chrysotile. Our findings thus indicate that the diffusion rates of a wide range of natural colloidal particles can be predicted from theory, so long as the particle aspect ratio is properly taken into account. This is an important first step for understanding aggregate formation and transport of non-spherical contaminant particles, in the environment and *in vivo*.

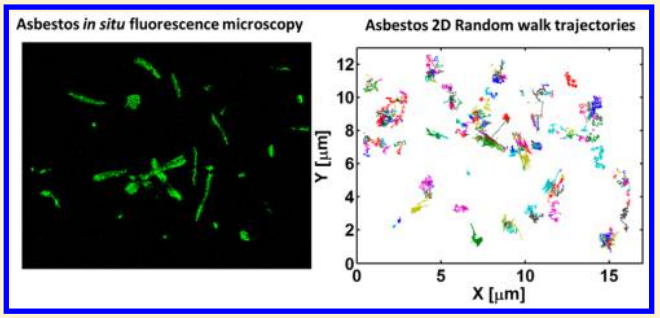

INTRODUCTION

The primary health impacts of exposure to fine particulates, such as asbestos fibers, are to the respiratory system, and therefore, inhalation of airborne particles is the exposure pathway of greatest concern. Accordingly, a substantial research effort has been made to understand the transport and dispersion of atmospheric particles, including asbestos fibers.[1−6]

Considerably less attention has been paid to the fate and transport of asbestos in aquatic environments, because (i) asbestos is generally considered safe in the aqueous phase and (ii) it has been assumed that mobility of asbestos in porous media is limited. However, there is mounting field evidence that asbestos fibers may be transported significant distances in groundwater,[7−9] representing a possibly significant but overlooked pathway for spreading of this hazardous material. In addition, numerous studies have indicated that the size of colloids exerts the primary control on their mobility and fate in the environment,[10−13] and there are indications that the length of asbestos fibers also influences toxicity.[14]

Brownian motion, wherein small particles suspended in a fluid undergo continuous random displacement, is essential to many industrial, environmental, and biological processes.[15−19] Predicting the diffusion of asbestos fibers in water would be an important step toward understanding asbestos mobility and retention in soils and the rate of formation of aggregates that may influence and even inhibit transport. It may also be relevant to understanding the behavior of asbestos in the body.[20] In the existing literature, asbestos fibers are commonly described as high aspect ratio rod-like particles,[21] and colloidal rods in liquids have been studied theoretically[18,22,23] and numerically[24,25] for decades. Recently, fluorescence video microscopy has allowed for direct experimental observation of the dynamics of rod-like colloids in water.[26−29] The groundbreaking study of Han et al.[18] reported theoretical predictions and experimental verification of the Brownian motion of an isolated and idealized ellipsoidal particle confined to two dimensions and elucidated the coupling between translational and rotational motion.

It is unclear whether predictions for single-particle diffusion of idealized Brownian rods are reliable for the less than ideal case of contaminants, such as asbestos, in a complex environment. Asbestos fibers have a large specific surface area, unique surface charge, and unusually large aspect ratio, and imperfections in the fiber structure could affect particle dynamics.[30,31] Moreover, asbestos fibers in the environment may occur in non-negligible concentrations and lie within pore spaces, both of which may produce confinement and

Received: August 8, 2015
Revised: October 5, 2015
Accepted: October 13, 2015
Published: October 13, 2015

DOI: 10.1021/acs.est.5b03839
Environ. Sci. Technol. 2015, 49, 13340−13349

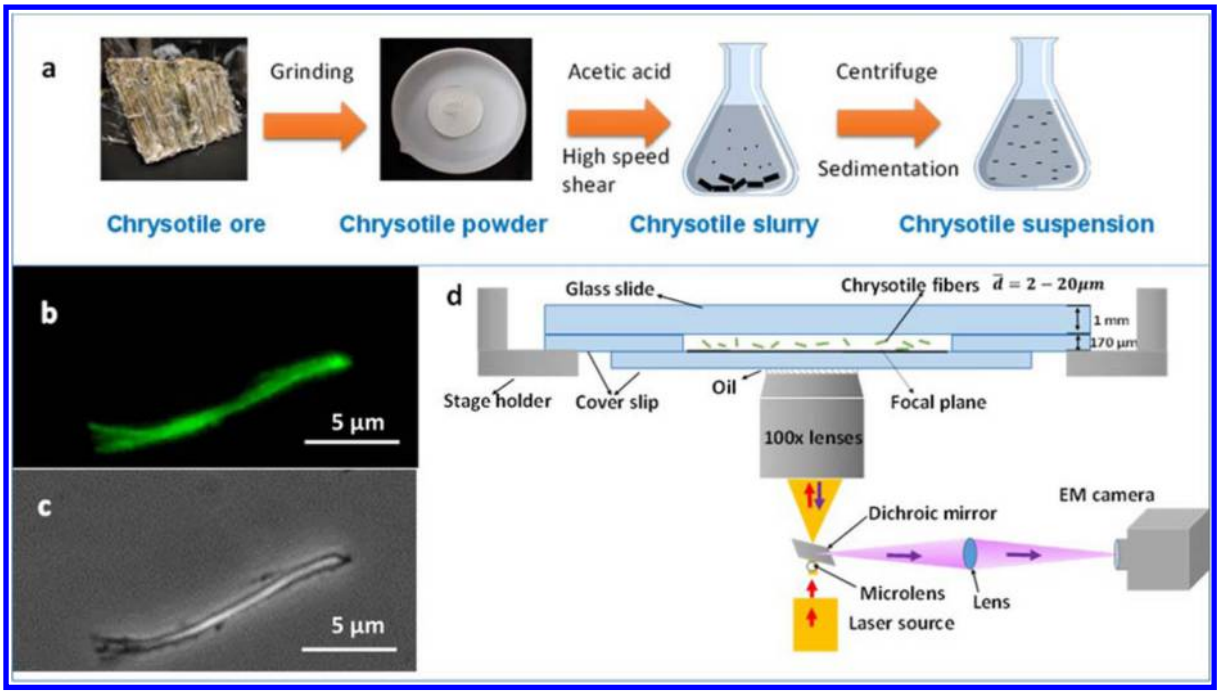

Figure 1. (a) Schematic of the procedure of producing stable chrysotile fiber suspension. (b and c) Comparison of (b) fluorescence microscopy and (c) phase contrast microscopy of single chrysotile fiber in water. Error bars represent 5 μm. (d) Schematic of the experiment: *in situ* liquid cell spinning-disk confocal microscopy.

interaction effects. In addition, there are challenges in experimentally observing the dynamics of asbestos fibers in the aqueous phase, because standard fluorescent dye does not bind to the surface of asbestos fibers and phase-contrast microscopy does not produce sufficient contrast. However, a recent study demonstrated that the DksA protein from *Escherichia coli* binds strongly and selectively to chrysotile, the most commonly used industrial form of asbestos, which now makes it possible to visualize the asbestos fibers in water by fluorescence microscopy.[4,32] In addition, the protein promotes stability of a chrysotile suspension by introducing steric repulsions between fibers.[33]

The objectives of this study are to (1) quantitatively characterize the translational and rotational diffusivity of asbestos fibers in water, to investigate the influence of the particle aspect ratio, and (2) test whether existing theory for Brownian rods can be used to describe these observations. We employ the recently developed fluorescent staining technique[32] to tag chrysotile fibers at batch scale and observe their diffusion in a liquid cell mounted on a spinning-disk confocal microscope. Automated elliptical particle detection[18] allows us to determine the dimensions, centroid, and orientation of each fiber in an image and to track the trajectories of these particles over time scales of 10^{-1}–10^{2} s. These data are used to compute the relevant quantities, mean square displacements (MSDs) and distributions of displacements, for testing diffusion theory. The range of asbestos particle lengths examined allows us to clearly demonstrate size-dependent diffusion. Results show that predictions from idealized Brownian motion are reasonably accurate, even for the case of complex particles at environmentally relevant concentrations. We discuss the significance of this finding for aggregate formation and environmental transport, for both asbestos in particular and elongated particles more generally.

MATERIALS AND METHODS

Sample Preparation and Fluorescent Tagging. Asbestos is a group of six fibrous silicate minerals that differ in their chemical composition, fiber shape, and toxicity.[34] Chrysotile, a member of the serpentine mineral group that accounts for more than 90% of industrial asbestos,[32] is the species used in this study. A raw chrysotile ore block (purity 90%) from El Dorado Mine, Salt River, Arizona, was used as the source material for generating fibers, while water used in experiments was treated with an Ultrapure Milli-Q system. Acetic acid and other electrolytes employed in some experiments (such as $KHCO_3$) were reagent-grade.

Our experimental solutions were prepared from aqueous suspension of raw chrysotile fibers at pH 6.9 using the method (Figure 1a) modified from an existing patent[35] for producing a stable suspension of finely divided chrysotile asbestos. The procedure is described as follows: First, 10 g of dry chrysotile ore is ground by a powder machine (SPEX MIXER/MILL model 8000, S/N 65777) for 30 min to open the bulk chrysotile fiber bundles from the ore. A 1 g sample of the mechanically opened chrysotile fibers (powder) is then added to a 2000 mL glass container, after which is added 1000 mL of water. Then, 0.5 mL of acetic acid (1 M) is added to the slurry, and a lab mixer (BenMix model OPLB-300) is turned on at high speed (about 10 000 rpm) and allowed to run for 3 min. The resulting asbestos dispersion is decanted into a 1000 mL tall-form beaker. Within 30 min after the dispersion is prepared, the largest fibers may settle out of the suspension. The supernatant is then decanted from the settled residue into a second beaker and centrifuged at 3000 rpm for 5 min. The supernatant from this treatment is decanted and discarded, and the remaining residue is dried and weighed. To produce chrysotile fiber suspensions at various concentrations, the appropriate weight of dry chrysotile fibers is dispersed with 1000 mL of water. Finally, an ultrasonic probe (Misonix Q55A)

DOI: 10.1021/acs.est.5b03839
Environ. Sci. Technol. 2015, 49, 13340−13349

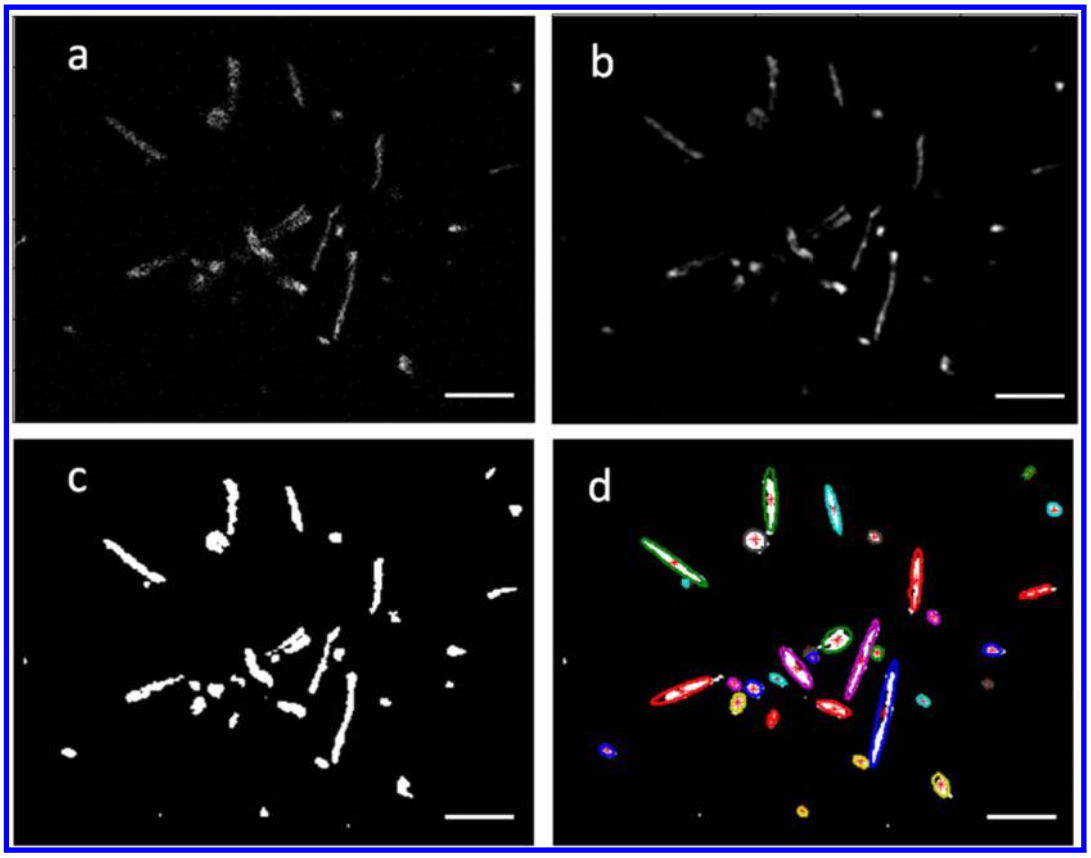

Figure 2. Fluorescence visualization of dynamics of individual chrysotile fibers in water. (a) Typical 2D view of the confocal image of diffusing fibers. (b) Image after filtering. (c) Converted binary image. (d) Identification of fiber centroids and shapes on the binary image. The elliptical shapes are color-coded to help distinguish between individual fibers. Scale bars are 10 μm.

is applied for 10 min just prior to the experiment, to redisperse the suspension. Using image analysis, we analyze the size distribution of all fibers at the beginning of each experiment (see below). Our results show that the procedure outlined here reliably produces well-dispersed fibers in the range of 1−20 μm.

Experiments were run at three different environmentally relevant concentrations, 20, 100, and 150 ppm, to determine empirically if particle diffusion is affected by the concentration. After redispersion, 40 μL of DksA−fluorescein probe reagent (probe amount is about 0.02 nmol, Siliconbio, Inc., Japan) is added to 5 mL of suspension to tag chrysotile fibers.

Liquid Cell Confocal Microscopy. Chrysotile fiber motions in water were recorded using a custom-made experimental setup (Figure 1d). In brief, the liquid cell was constructed by mounting a coverslip on a glass slide. The glass surfaces were cleaned in a 1:4 mixture of hydrogen peroxide and sulfuric acid and by application of ultrasonication. Typically, 1 μL of asbestos suspension was spread over the entire coverslip area; it was observed that asbestos fibers did not stick to the surfaces. The cell was sealed with ultraviolet (UV)-cured adhesive (Norland 65, Edmund Optics, Barrington, NJ) to prevent convective flow as a result of evaporation. At least 10 min was allowed between sealing of the sample and image acquisition to ensure the cessation of any convective flow induced by the preparation procedure. The average gap between the glass slide and the coverslip was measured as 170 ± 2 μm. Images were acquired on a spinning-disk confocal microscope (Olympus IX81 inverted system) with fluorescein isothiocyanate (FITC) filter cube (λ_{ex}, 488 nm; λ_{em}, 520 nm), a 100× oil-immersion objective [numerical aperture (NA), 1.4; depth of focus, 0.5 μm], and a Andor iXon3 electron-multiplying charge-coupled device (EMCCD) camera (10 frames per second) controlled by MetaMorph software (Universal Imaging Co., Downingtown, PA). Images were collected at a fixed-elevation plane approximately 8−10 μm above the coverslip to minimize the magnitude of wall hydrodynamic interactions (Figure 1d).

Image Analysis. Images are processed using a morphological image processing algorithm reported by Han et al.,[18] to identify particles using best-fit ellipses and track their motion (Figure 2). In brief, the first step is to read source images, which are two-dimensional (2D) slices (in a plane parallel to the coverslip) of the liquid cell (Figure 2a). We then implement a real-space bandpass filter, which suppresses pixel noise and long-wavelength image variations while retaining information on a characteristic size (Figure 2b). After filtering, we apply a threshold method to generate binary images (Figure 2c). The typical value for the threshold is between 2 and 2.5 pixels and can be determined by a quick test on a single image in an image processing program, such as ImageJ. After groups of pixels most likely belonging to a single fiber are indexed, we use the built-in 2D "regionprops" function in MATLAB to locate the center and orientation of the fibers in each frame. An elliptical shape is then fit to these fibers (Figure 2d). From this procedure, we obtain data on the center of mass in the lab frame, orientation angle, and major and minor axis length for each particle in an image. Displacements of the centroid locations of individual fibers are tracked and compared from one frame to the next to yield trajectory linking;[36] a fiber in the time frame j is linked to a fiber from the time frame $(j - 1)$ if the change in the centroid

DOI: 10.1021/acs.est.5b03839
Environ. Sci. Technol. 2015, 49, 13340−13349

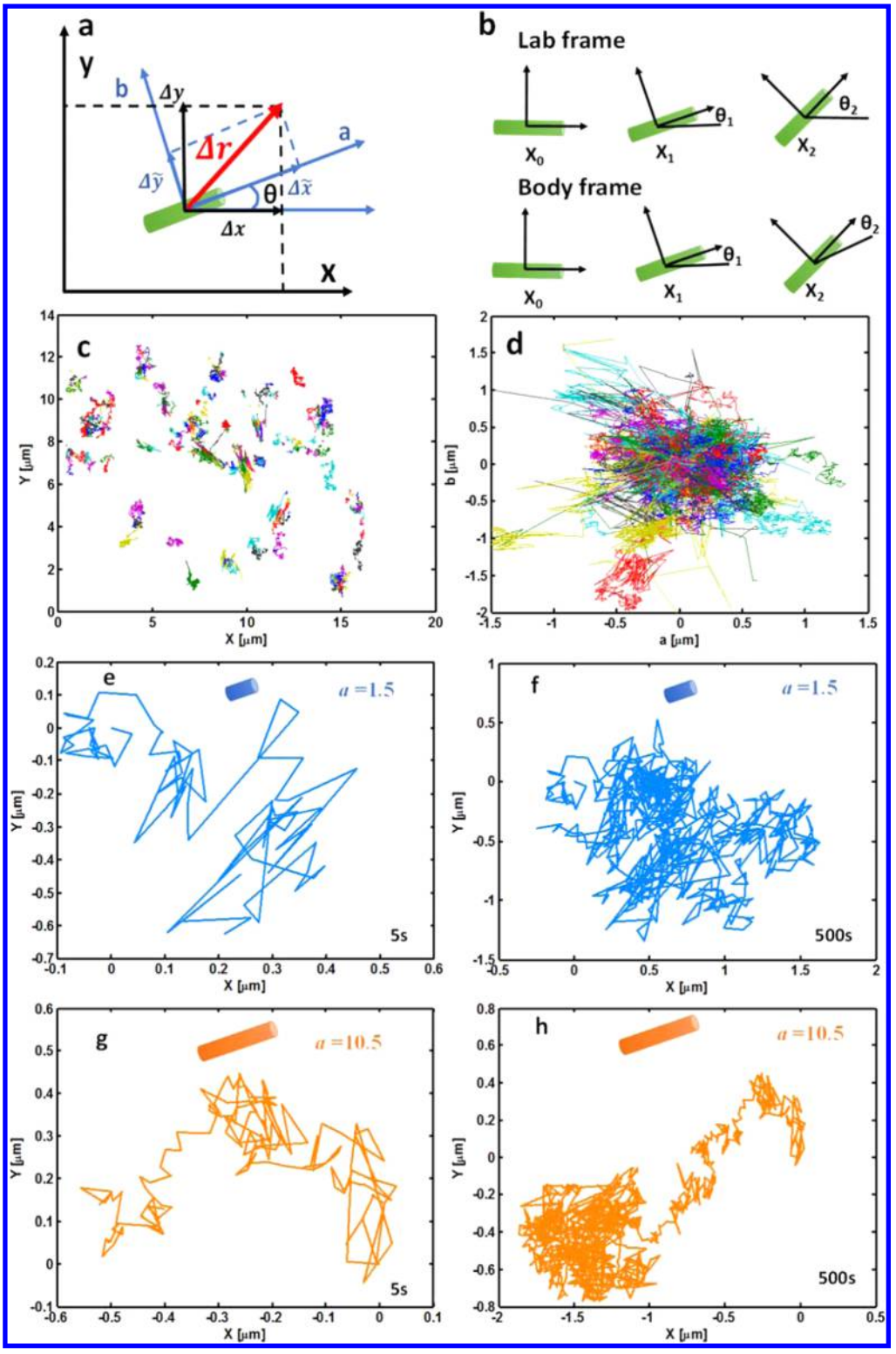

Figure 3. Experimental measurement on a dilute suspension of chrysotile fibers with various aspect ratios in water. The chrysotile fiber concentration equals 100 ppm. (a) Representation of a chrysotile fiber in the $x-y$ lab frame and the $a-b$ body frame. The angle between the two frames is θ. The displacement Δr can be decomposed as $(\Delta x, \Delta y)$ or $(\Delta\tilde{x}, \Delta\tilde{y})$. (b) Defining trajectories by lab-frame and body-frame displacement measurements. (c) Lab-frame and (d) body-frame 2D 100 s random walk trajectories of diffusing chrysotile fibers with various aspect ratios. (e and f) Random walk trajectory of a typical short chrysotile fiber during 5 and 500 s. (g and h) 2D random walk trajectory of a typical long chrysotile fiber during 5 and 500 s, respectively. Note the anisotropic behavior at short time scales (g), as shown by larger displacement in the x direction compared to the y direction; diffusion becomes isotropic at later times (h).

location is less than its smallest dimension. The consistent color coding between the frames identifies individual fiber trajectories (Figure 3c). It is important to note here that our measurements tracked the motion of individual fibers. Although aggregation

DOI: 10.1021/acs.est.5b03839
Environ. Sci. Technol. 2015, 49, 13340−13349

can occur in this system, the process is slow compared to the time scale of observation for the reported experiments. We measured the particle size distribution throughout the experiment to confirm that there was no significant change.

Brownian Motion Measurement and Theory. It is important to note that, although we characterize the motion of chrysotile fibers in 2D, these fibers are diffusing in a three-dimensional (3D) volume and, thus, are capable of moving into and out of the visualized slice. Measured diffusivities will thus vary from their true value by a small but unknown amount, and this should be kept in mind when 2D Brownian motion predictions are compared to our data. We return to this idea in the Discussion.

We first consider lab-frame characterization. After the image analysis, for each fiber, we obtain data consisting of centroid positions $x(t_n) = [x(t_n), y(t_n)]$ and orientation angles θ_n relative to the x axis at times $t_n = n(1/10)s$, where $(1/10)s$ is defined as a step. During the nth step, the position of the fibers changes by $\delta x(t_n) = x(t_n) - x(t_{n-1})$ and its orientation angle changes by $\delta\theta(t_n) = \theta(t_n) - \theta(t_{n-1})$. From the data set, we extracted an ensemble of chrysotile fiber trajectories starting at different times t and ending at time τ_0 later. The total positional and angular displacements in these trajectories are $\Delta x(t) = x(t + \tau_0) - x(t)$ and $\Delta\theta(t) = \theta(t + \tau_0) - \theta(t)$, respectively (Figure 3b). The minimum time step, $^1/_{10}$ s, was set by the camera frame rate, while the maximum observation time (approximately 100 s) was determined by the limited size of the observation window.

We then consider the translational motion of chrysotile fibers by decomposing the displacement δx_n into its components δx_{ni} relative to the fixed lab frame and $\delta\tilde{x}_{ni}$ relative to the body frame. As shown in Figure 3a, the two are related via a rotation, $\delta\tilde{x}_{ni} = R_{ij}\ \delta x_{nj}$, where $R_{ij} = \begin{pmatrix} \cos\theta_n & \sin\theta_n \\ -\sin\theta_n & \cos\theta_n \end{pmatrix}$ is the rotation matrix with $\theta_n = [\theta(t_{n-1}) + \theta(t_n)]/2$. We constructed total body-frame displacement by summing over displacement in each step, $\tilde{x}(t_n) = \sum_{k=1}^{n}\delta\tilde{x}_k$, and from this, we can construct body-frame displacement for trajectories of duration t at starting time τ_0 via $\Delta\tilde{x}(t) = \tilde{x}(t + \tau_0) - \tilde{x}(\tau_0)$. The standard error is estimated from the standard deviation of displacements in each step divided by the square root of the number of observed fibers.

MSDs in the body frame and in the lab frame, averaged over all trajectories, can be written as eqs 1, 2, and 3, respectively

$$\langle[\Delta\tilde{x}(t)]^2\rangle = 2D_a t, \qquad \langle[\Delta\tilde{y}(t)]^2\rangle = 2D_b t \tag{1}$$

$$\langle[\Delta x(t)]^2\rangle = 2D_x t, \qquad \langle[\Delta y(t)]^2\rangle = 2D_y t \tag{2}$$

$$\langle[\Delta x(t)]^2\rangle + \langle[\Delta y(t)]^2\rangle = 4D_{xy} t \tag{3}$$

where D_a and D_b are the one-dimensional (1D) diffusion coefficients along the a and b axes in the body frame, respectively. The parameters D_x and D_y are the 1D diffusion coefficients along the x and y axes in the lab frame, respectively. D_{xy} is the 2D diffusion coefficient in the lab frame.

Theoretically, chrysotile fibers can be modeled as rigid rods with large aspect ratios, for which diffusion theory is well-developed.[26,28,37,38] The 2D translational diffusion coefficient is predicted from theory[38] to be

$$D_{xy} = \frac{k_B T}{6\pi\eta_s}\frac{2\ln(L/d) - \gamma_{\parallel} - \gamma_{\perp}}{L} \tag{4}$$

where k_B is the Boltzmann constant, T is the sample temperature (296 K in our experiments), η_s is the solution viscosity (1.0 ± 0.1 mPa s), and $\gamma_{\parallel}$ (-0.11) and $\gamma_{\perp}$ (0.89) are end correction coefficients,[38] d is the effective chrysotile fiber diameter, and L is the fiber length. The length of chrysotile fibers in our samples varies from 1 to 20 μm, whereas their effective diameters, including the protein-based probe coating, were estimated to fall within the narrow range of 1.5 ± 0.5 μm.

We then consider the statistical properties of $\Delta\theta(t)$, which is expected to be independent of translational motions.[18] For a free chrysotile fiber, MSDs of angle $\langle[\Delta\theta(t)]^2\rangle$ can be written as

$$\langle[\Delta\theta(t)]^2\rangle = 2D_\theta t \tag{5}$$

where D_θ is the 1D rotational diffusion coefficient.

According to the theory of Broersma,[37] the rotational diffusion coefficient D_θ of a rigid rod is predicted to be

$$D_\theta = \frac{3k_B T}{\pi\eta_s}\frac{\ln(L/d) - \gamma_r}{L^3} \tag{6}$$

where γ_r (-0.45) is a length-dependent end-correction coefficient.[37]

We now turn to the body- and lab-frame probability distributions of translational displacements. According to the study by Han et al.,[18] the probability distribution function (PDF) for body-frame displacements $\Delta\tilde{x}_i(t)$ is Gaussian and can be written as

$$f(\Delta\tilde{x}_i, t) = \frac{1}{\sqrt{2\pi}\,\sigma_i(t)}\, e^{\Delta\tilde{x}_i^2/2\sigma^2{}_i(t)} \tag{7}$$

where $\sigma^2{}_i(t) = 2D_i t$ and $D_i = (D_a, D_b)$.

Although the work by Han et al. shows that PDFs of displacement in the lab frame exhibit non-Gaussian behavior in the tails at short time scales, a Gaussian fit provides a first-order approximation. In this study, we assume that the PDFs of displacement in the lab frame also follow Gaussian behavior.

One consequence of a large aspect ratio is that, at short time scales, particles have a tendency to diffuse more rapidly along their axis (a direction) than orthogonal to it as a result of hydrodynamic effects.[18] Accordingly, diffusion of large aspect ratio rods appears to be anisotropic over short time scales, which is visually apparent in particle trajectories that show correlations at short time scales; particle rotation eventually drives a crossover to isotropic diffusion at sufficiently long time scales, when memory of the orientation is lost.[18] This effect should be apparent in the distribution of particle displacements in the body frame,[18] where we expect along axis displacements to be larger.

RESULTS

2D Random Walk Trajectories. Quantification of chrysotile fiber Brownian motion is shown in Figure 3. Figure 3c (lab frame) and Figure 3d (body frame) plot displacement of hundreds of chrysotile fibers during a representative experiment (100 s). The results indicate that the chrysotile fibers undergo significant displacement when they diffuse in water. A qualitative but important observation is that the chrysotile fibers exhibit the expected effect of the particle length on diffusion. Small aspect ratio particles exhibit isotropic diffusion over the entire range of observation (Figure 3e). Elongated particles, however, diffuse anisotropically at short time scales as a result of their tendency for along axis motion

DOI: 10.1021/acs.est.5b03839
Environ. Sci. Technol. 2015, 49, 13340−13349

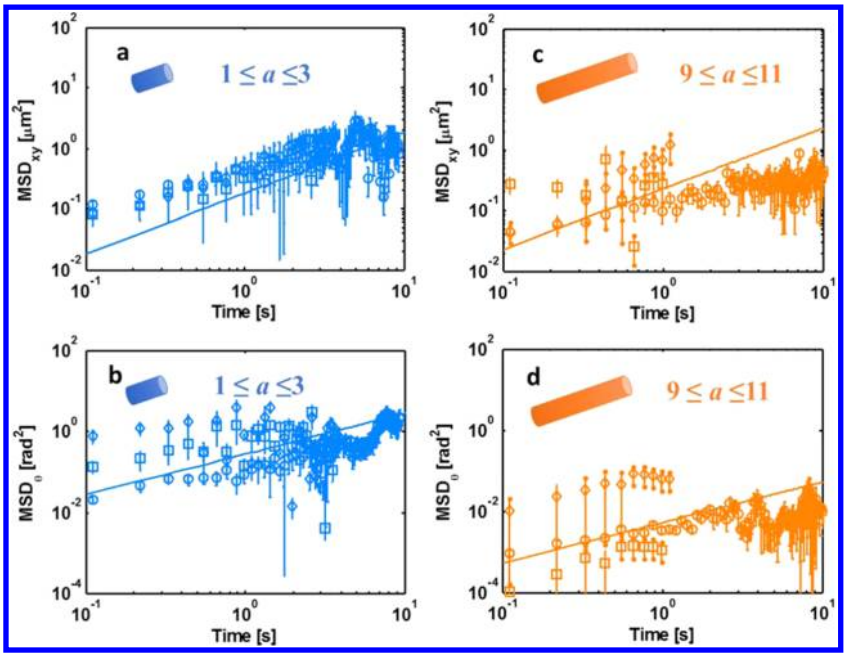

Figure 4. MSD graphs computed from trajectories of thousands of individual chrysotile fibers at different initial concentrations (◇, 20 ppm; ○, 100 ppm; and □, 150 ppm). (a and c) Translational MSDs of short (blue) and long (orange) chrysotile fibers, respectively. (b and d) Rotational MSDs of short (blue) and long (orange) chrysotile fibers, respectively. Open symbols represent experimental observations, and solid lines represent theoretical values. See Figure S1 of the Supporting Information for plots of all aspect ratio classes.

Table 1. Comparison between Experimental and Theoretical Values of Translational (D_{xy}) and Rotational (D_θ) Diffusion Coefficients for Chrysotile Fibers with Various Aspect Ratios[a]

aspect ratio	D_{xy} ($\mu m^2/s$)	D_θ (rad^2/s)
$1 \geq a \geq 3$	$9.6 \times 10^{-2} \pm 4.1 \times 10^{-2}$ (8.2×10^{-2})	$2.3 \times 10^{-1} \pm 3.3 \times 10^{-2}$ (1.3×10^{-1})
$3 \geq a \geq 5$	$1.2 \times 10^{-1} \pm 2.2 \times 10^{-2}$ (7.7×10^{-2})	$3.1 \times 10^{-2} \pm 1.3 \times 10^{-2}$ (2.7×10^{-2})
$5 \geq a \geq 7$	$5.6 \times 10^{-2} \pm 1.3 \times 10^{-2}$ (7.0×10^{-2})	$2.2 \times 10^{-3} \pm 8.8 \times 10^{-4}$ (9.8×10^{-3})
$7 \geq a \geq 9$	$4.1 \times 10^{-2} \pm 9.1 \times 10^{-3}$ (6.1×10^{-2})	$1.3 \times 10^{-3} \pm 3.4 \times 10^{-4}$ (4.7×10^{-3})
$9 \geq a \geq 11$	$3.7 \times 10^{-2} \pm 6.8 \times 10^{-3}$ (5.4×10^{-2})	$9.0 \times 10^{-4} \pm 3.6 \times 10^{-4}$ (2.6×10^{-3})

[a]Values in parentheses are theoretical predictions.

(Figure 3g). At sufficiently long time scales, diffusion of these elongated particles crosses over to isotropic behavior as a result of rotation, which washes out the directional memory of the random walk (Figure 3h).

MSD of Translational and Rotational Diffusion. We computed the translational MSDs for thousands of chrysotile fibers with various aspect ratios under the three different concentrations (20, 100, and 150 ppm) and compared these results to the corresponding theoretical predictions for single-particle diffusion of Brownian rods (Figure 4 and Figure S1 of the Supporting Information). The 2D diffusion coefficients can be obtained empirically using eq 3, once the respective MSDs are calculated. These diffusion coefficients are reported in Table 1. The corresponding theoretical diffusion coefficients are calculated using eq 4. The growth of the MSD with time is consistent with a linear form and, hence, diffusion for all of the data, although with significant variance (panels a and c of Figure 4 and Figure S1 of the Supporting Information). The deviations between experimentally determined and theoretically predicted diffusivities are small (by a factor of 2). Translational diffusivities are size (length) dependent; however, the effect is mild (see eq 4) and appears to be taken into account by the theory (Figure S1 of the Supporting Information). Much of the variance in the data appears to be due to concentration, an effect not considered in the theory, which assumes single-particle diffusion.

Similarly, we report the rotational MSDs and corresponding theoretical predictions for the same experiments (panels b and d of Figure 4 and Figure S1 of the Supporting Information). Theoretical predictions for the rotational diffusion coefficient D_θ (eq 6) indicate an inverse cubic dependence of length. Our experimental results confirm this trend. In comparison to translational diffusion, however, the difference between theoretical and experimental diffusivities for rotation has a larger range (by a factor of 4), and the data also exhibit greater variability and perhaps a larger influence of concentration. Larger variability in rotational data is not surprising, because the angle resolution is significantly worse than detection of the centroid in the ellipse-fitting scheme; this is a consequence of spatial and temporal variations in particle brightness and movement in and out of the focal plane (Movie S2 of the Supporting Information).

PDF of Displacement. We measured the distribution of particle displacements along a coordinate axis in a time interval t. As discussed in the theory section, the PDF for displacements in the lab and body frames is predicted to be Gaussian (or near Gaussian), and the data are indeed reasonably well fit by a Gaussian distribution (Figure 5). More quantitatively, the standard deviation of each PDF should be directly related to

DOI: 10.1021/acs.est.5b03839
Environ. Sci. Technol. 2015, 49, 13340−13349

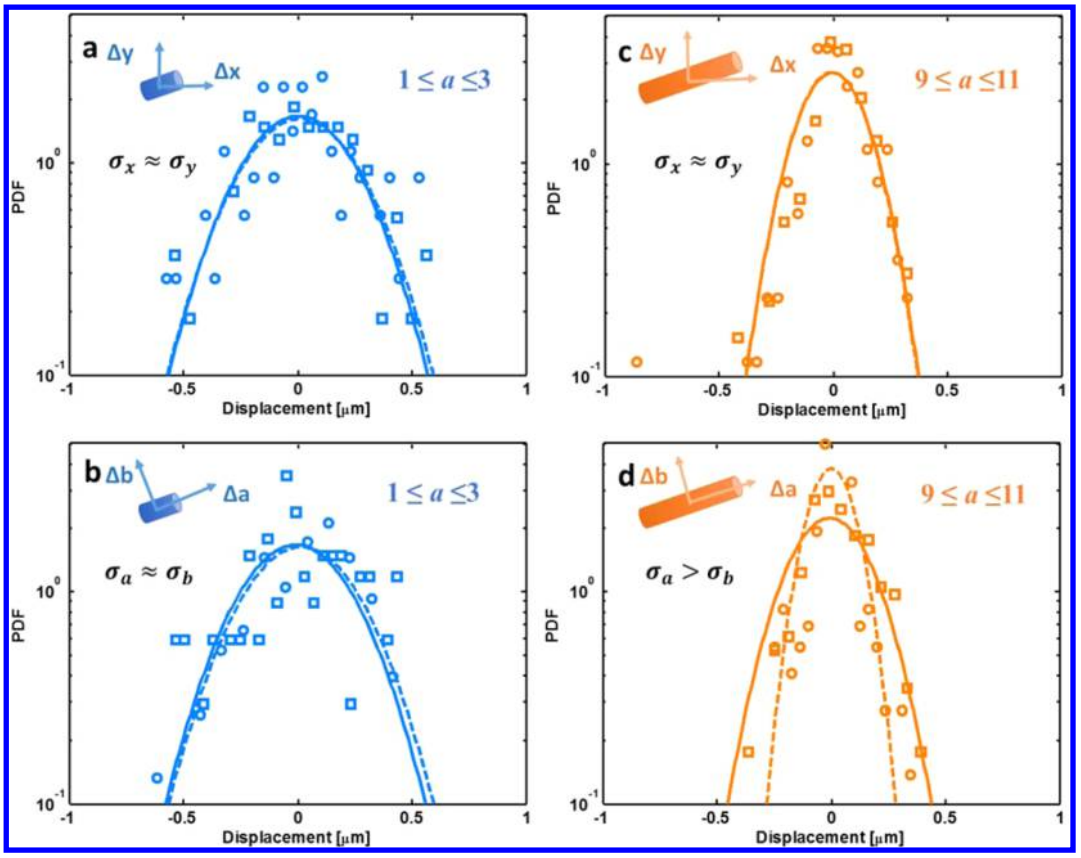

Figure 5. Probability distributions of displacements measured over t = 0.1 s, for an experiment with a chrysotile fiber concentration of 100 ppm. (a and c) Lab-frame PDFs for (□) Δx and (○) Δy, respectively. (b and d) Body-frame PDFs for (□) $\Delta\tilde{x}$ and (○) $\Delta\tilde{y}$, respectively. (—) Best Gaussian fit for Δx or $\Delta\tilde{x}$. (- - -) Best Gaussian fit for Δy or $\Delta\tilde{y}$. For body-frame, $D_a = 9.4 \times 10^{-2}$ and 7.2×10^{-2} $\mu m^2/s$ for short and long chrysotile fibers, respectively, and $D_b = 9.0 \times 10^{-2}$ and 1.1×10^{-2} $\mu m^2/s$ for short and long chrysotile fibers, respectively. For lab-frame, $D_x = 9.8 \times 10^{-2}$ and 4.6×10^{-2} $\mu m^2/s$ for short and long chrysotile fibers, respectively, and $D_y = 9.3 \times 10^{-2}$ and 4.4×10^{-2} $\mu m^2/s$ for short and long chrysotile fibers, respectively. Data indicate isotropic diffusion for short (equant) particles and anisotropic diffusion with larger along axis displacements for elongated particles.

diffusivity through eqs 1 and 2, where the 2D diffusivity may be computed from the measured 1D distributions as $D_{xy} = (D_x + D_y)/2 = (D_a + D_b)/2$. Thus, fitting a Gaussian distribution to the displacement data provides an independent estimate of diffusivity. Indeed, empirically determined diffusivities from the Gaussian fits are in reasonable agreement with those determined from the MSDs (Figure 5; by a factor of 3). The data also confirm the following expectations from theory: PDFs indicate isotropic diffusion in the lab frame for short and long particles (particles should have no preferred direction of motion in the Cartesian frame; panels a and c of Figure 5); lab- and body-frame PDFs are identical for short particles (panels a and b of Figure 5); i.e., there is no preferred direction of motion for equant particles; and body-frame PDFs show that elongated particles have larger displacements along axis at short times (Figure 5d); i.e., they exhibit anisotropic diffusion. Our longest particles have an aspect ratio of order 10, and the displacement PDFs indicate a diffusion anisotropy of $D_a/D_b \approx 6$ at a time scale Δt = 0.1 s. This is comparable in magnitude to the observed anisotropy for particles of a similar aspect ratio reported by Han et al.[18] From theory, we expect that the time scale over which diffusion becomes isotropic is determined by the rotational diffusion time (i.e., the time to "lose" memory of orientation) and should scale with the aspect ratio cubed; for our particles with an aspect ratio of 10, this is of order 10 s, consistent with our observations. See the study by Han et al.[18] for a more detailed treatment.

DISCUSSION

We have used spinning-disk confocal microscopy to track the diffusion of fluorescent-tagged chrysotile asbestos fibers in water at environmentally relevant concentrations. Our observations demonstrate that the theories of single-particle Brownian motion of rods[18,37] predict, to first order, the translational and rotational dynamics observed in our system. There are significant discrepancies between our measurements and theoretical predictions; however, we consider here some possible explanations for these differences. First, there are several possible sources of measurement error that could be important but are not quantified at present. One of them is related to dimensionality; because the asbestos fibers actually undergo 3D diffusion while we only track 2D motion in a plane, experimental measurements likely underestimate true diffusivity, which results in a discrepancy with (2D) theoretical predictions. Another source of potential error is that fibers can move in and out of the focal plane, which introduces errors in determination of the position. Determination of rotational motion is significantly more error-prone than translation, because fitted ellipse size fluctuates more than centroid position when particles move in and out of the focal plane. Lastly, imperfections of the chrysotile fibers may cause uneven coating

DOI: 10.1021/acs.est.5b03839
Environ. Sci. Technol. 2015, 49, 13340−13349

of the fluorescence dye on the surfaces, which may lead to error in identification and characterization of the fibers. Besides error, there appears to be a real effect of the concentration on particle diffusivity in the experiments. The MSD plots for all fiber lengths show that data are stratified by the concentration (Figure 4 and Figure S1 of the Supporting Information). Although the data are variable, the general trend is that translational and rotational diffusion decrease as the concentration increases. This intuitively makes sense, because it indicates that fiber motion slows as the particles become crowded.[16,39] However, a simple model for volume exclusion effects[40] predicts that the influence of the concentration should be negligible for all of our experiments, suggesting that hydrodynamic interactions may be relevant. Thus, while the linear increase of MSD with time indicates generally diffusive behavior for all concentrations, it appears that increasing the concentration from 20 to 150 ppm results in a modest change in the rate of particle diffusion, somehow as a result of particle−particle interactions. Quantifying this effect would require experiments over a significantly larger range of concentrations; however, it is challenging to significantly increase the concentration because the optics are degraded as a result of light attenuation.

In addition, besides error, previous experimental studies of the diffusivity of spheres have shown that the 2D diffusivity deviates systematically from the 3D diffusivity, except in the limit of dilute suspensions, far from a wall.[41] The dynamical deviations from bulk diffusion for rods near a rigid boundary should produce measurable entropic forces,[42] resulting from interactions between the rods and the walls. These types of interactions may be important to explore in future studies of the transport of colloidal rods through a porous medium, where the rods would necessarily come into contact with walls at larger particle concentrations.

Environmental Implications. Although the theory for Brownian motion of rods is well-known, up to now, it has only been experimentally tested for synthetic and well-controlled elongated particles under highly idealized experimental conditions. While our liquid cell experiment is a far cry from the complexity of the natural environment, it does include natural and (presumably) compositionally variable material, a wide distribution of particle lengths and (presumably) shapes, and significant particle concentrations. In addition, as far as we know, the longest particles in our experiments possess an aspect ratio larger than any previous study and, therefore, extend the known range of applicability of the Brownian rod approximation. This study provides a building block toward predicting the diffusion of asbestos fibers in the natural environment. The success of the diffusion theory in describing our experiments, with no calibration, indicates that it may also be employed to describe the diffusion of asbestos and other fibers in the more viscous physiological fluids of the human lung or porous solids. Specifically, eqs 4 and 6 account for the effects of fluid density and temperature, in addition to particle size and shape. We suggest that this diffusion theory should be broadly applicable to a wide range of colloids and environments.

In many situations, even airborne asbestos particles will have spent a significant time in partially or fully saturated soil before entrainment by the wind; thus, the dynamics of asbestos in the aqueous phase cannot be ignored. Although molecular diffusion is typically small compared to the magnitudes of large-scale contaminant advection and dispersion, diffusion is important for several reasons. It can influence the sorption and retention of colloidal particles in porous media.[43,44] Diffusion may be relevant for how asbestos fibers migrate within the lung.[45,46] Anisotropic diffusion also raises some interesting questions about how and whether particle orientation influences mobility in confined areas, such as soil pores. Under the presence of a shear flow, elongated particles will orient themselves to align with vorticity at a sufficiently large rotational Peclet number ($Pe_r = \dot{\gamma}/D_r$, where $\dot{\gamma}$ is the shear rate and D_r is the rotational diffusion coefficient).[47] For a given elongated particle ($l = 1 \times 10^{-5}$ m, and $D_r = 1 \times 10^{-3}$ rad/s) under typical groundwater flow conditions ($v = 1 \times 10^{-6}$ m/s, and $r = 1 \times 10^{-3}$ m), $Pe_r \sim 1$. This simple scale analysis indicates that fluid advection and molecular diffusion may both have a significant influence on particle rotation; how these effects control the movement of rods through pore throats is worthy of further attention.

Finally and perhaps most importantly, diffusion sets the pace of aggregate growth by determining the collision frequency of particles.[48−50] Because virtually all colloids form aggregates[44,51−53] and the size of aggregates determines the mobility of particles in air,[3] streams,[54] and groundwater,[10,11] knowing the rate of diffusion is a key first step toward a more mechanistic understanding of colloidal transport in the environment. It is possible that idealized models for aggregate growth[48,55] may be generalized to environmentally relevant materials and settings. This next step, however, requires a better understanding of particle−particle interactions. The anisotropic nature of diffusion for rods may influence these interactions by determining particle contact geometry, with implications for both aggregate structure and kinetics. This effect remains to be explored.

■ ASSOCIATED CONTENT

Supporting Information

The Supporting Information is available free of charge on the ACS Publications website at DOI: 10.1021/acs.est.5b03839.

Fluorescence microscopy of chrysotile fiber diffusing in water (Movie S1) (AVI)

Fluorescence microscopy of chrysotile fiber diffusing in water with ellipsoidal particle tracking (Movie S2) (AVI)

Translational and rotational MSDs computed from trajectories of chrysotile fibers with various aspect ratios and the corresponding theoretical predictions (Figure S1) (PDF)

■ AUTHOR INFORMATION

Corresponding Author

*Telephone: 215-746-2813. Fax: 215-898-0964. E-mail: sediment@sas.upenn.edu.

Notes

The authors declare no competing financial interest.

■ ACKNOWLEDGMENTS

This research is fully supported by the National Institute of Environmental Health Sciences (NIEHS) through Superfund Grant P42ES 23720.

■ REFERENCES

(1) Ostro, B. D.; Hurley, S.; Lipsett, M. J. Air pollution and daily mortality in the coachella valley, california: A study of pm10 dominated by coarse particles. *Environ. Res.* **1999**, *81*, 231−238.

DOI: 10.1021/acs.est.5b03839
Environ. Sci. Technol. 2015, 49, 13340−13349

(2) Malcolm, A. L.; Derwent, R. G.; Maryon, R. H. Modelling the long-range transport of secondary pm10 to the uk. *Atmos. Environ.* **2000**, *34*, 881−894.
(3) Kok, J. F. A scaling theory for the size distribution of emitted dust aerosols suggests climate models underestimate the size of the global dust cycle. *Proc. Natl. Acad. Sci. U. S. A.* **2011**, *108*, 1016−1021.
(4) Ishida, T.; Alexandrov, M.; Nishimura, T.; Minakawa, K.; Hirota, R.; Sekiguchi, K.; Kohyama, N.; Kuroda, A. Selective detection of airborne asbestos fibers using protein-based fluorescent probes. *Environ. Sci. Technol.* **2010**, *44*, 755−759.
(5) Kurumatani, N.; Kumagai, S. Mapping the risk of mesothelioma due to neighborhood asbestos exposure. *Am. J. Respir. Crit. Care Med.* **2008**, *178*, 624−629.
(6) Gopalakrishnan, R.; McMurry, P. H.; Hogan, C. J., Jr The electrical mobilities and scalar friction factors of modest-to-high aspect ratio particles in the transition regime. *J. Aerosol Sci.* **2015**, *82*, 24−39.
(7) Burkhardt, M.; Kasteel, R.; Vanderborght, J.; Vereecken, H. Field study on colloid transport using fluorescent microspheres. *European Journal of Soil Science* **2008**, *59*, 82−93.
(8) Koumantakis, E.; Kalliopi, A.; Dimitrios, K.; Gidarakos, E. Asbestos pollution in an inactive mine: Determination of asbestos fibers in the deposit tailings and water. *J. Hazard. Mater.* **2009**, *167*, 1080−1088.
(9) Buck, B. J.; Goossens, D.; Metcalf, R. V.; McLaurin, B.; Ren, M.; Freudenberger, F. Naturally occurring asbestos: Potential for human exposure, southern nevada, USA. *Soil Science Society of America Journal* **2013**, *77*, 2192−2204.
(10) Ryan, J. N.; Elimelech, M. Colloid mobilization and transport in groundwater. *Colloids Surf., A* **1996**, *107*, 1−56.
(11) Bradford, S. A.; Simunek, J.; Bettahar, M.; Van Genuchten, M. T.; Yates, S. R. Modeling colloid attachment, straining, and exclusion in saturated porous media. *Environ. Sci. Technol.* **2003**, *37*, 2242−2250.
(12) Lin, H.-K.; Pryadko, L. P.; Walker, S.; Zandi, R. Attachment and detachment rate distributions in deep-bed filtration. *Phys. Rev. E* **2009**, DOI: 10.1103/PhysRevE.79.046321.
(13) Wang, Y.; Gao, B.; Morales, V. L.; Tian, Y.; Wu, L.; Gao, J.; Bai, W.; Yang, L. Transport of titanium dioxide nanoparticles in saturated porous media under various solution chemistry conditions. *J. Nanopart. Res.* **2012**, DOI: 10.1007/s11051-012-1095-y.
(14) Quinn, M. M.; Smith, T. J.; Ellenbecker, M. J.; Wegman, D. H.; Eisen, E. A. Exposure assessment for airborne man-made mineral fibers - some comments. *Ann. Occup. Hyg.* **1994**, *38*, 959−961.
(15) McCarthy, J. F.; Zachara, J. M. Subsurface transport of contaminants - mobile colloids in the subsurface environment may alter the transport of contaminants. *Environ. Sci. Technol.* **1989**, *23*, 496−502.
(16) Roosen-Runge, F.; Hennig, M.; Zhang, F.; Jacobs, R. M. J.; Sztucki, M.; Schober, H.; Seydel, T.; Schreiber, F. Protein self-diffusion in crowded solutions. *Proc. Natl. Acad. Sci. U. S. A.* **2011**, *108*, 11815−11820.
(17) Röcker, C.; Pötzl, M.; Zhang, F.; Parak, W. J.; Nienhaus, G. U. A quantitative fluorescence study of protein monolayer formation on colloidal nanoparticles. *Nat. Nanotechnol.* **2009**, *4*, 577−580.
(18) Han, Y.; Alsayed, A. M.; Nobili, M.; Zhang, J.; Lubensky, T. C.; Yodh, A. G. Brownian motion of an ellipsoid. *Science* **2006**, *314*, 626−630.
(19) Saffman, P. G.; Delbruck, M. Brownian-motion in biological-membranes. *Proc. Natl. Acad. Sci. U. S. A.* **1975**, *72*, 3111−3113.
(20) Lippmann, M. Effects of fiber characteristics on lung deposition, retention, and disease. *Environ. Health Perspect.* **1990**, *88*, 311.
(21) Murai, Y.; Kitagawa, M.; Matsui, K.; Koizumi, F.; Miwa, A. Asbestos fiber analysis in 9 lung-cancer cases with high asbestos exposure. *Arch. Environ. Health* **1995**, *50*, 320−325.
(22) Furry, W. H. Isotropic rotational brownian motion. *Phys. Rev.* **1957**, *107*, 7−13.
(23) Onsager, L. The effects of shape on the interaction of colloidal particles. *Ann. N. Y. Acad. Sci.* **1949**, *51*, 627−659.
(24) Koike, O.; Ohta, S.; Fujita, M.; Yamaguchi, Y. Simulation model of concentrated colloidal rod-like nanoparticles. *Jpn. J. Appl. Phys.* **2008**, *47*, 8124−8130.
(25) Winkler, R. G.; Mussawisade, K.; Ripoll, M.; Gompper, G. Rod-like colloids and polymers in shear flow: A multi-particle-collision dynamics study. *J. Phys.: Condens. Matter* **2004**, *16*, S3941−S3954.
(26) Duggal, R.; Pasquali, M. Dynamics of individual single-walled carbon nanotubes in water by real-time visualization. *Phys. Rev. Lett.* **2006**, DOI: 10.1103/PhysRevLett.96.246104.
(27) Mukhija, D.; Solomon, M. J. Translational and rotational dynamics of colloidal rods by direct visualization with confocal microscopy. *J. Colloid Interface Sci.* **2007**, *314*, 98−106.
(28) Tsyboulski, D. A.; Bachilo, S. M.; Kolomeisky, A. B.; Weisman, R. B. Translational and rotational dynamics of individual single-walled carbon nanotubes in aqueous suspension. *ACS Nano* **2008**, *2*, 1770−1776.
(29) Marshall, B. D.; Davis, V. A.; Lee, D. C.; Korgel, B. A. Rotational and translational diffusivities of germanium nanowires. *Rheol. Acta* **2009**, *48*, 589−596.
(30) van Bruggen, M. P. B.; Lekkerkerker, H. N. W.; Maret, G.; Dhont, J. K. G. Long-time translational self-diffusion in isotropic and nematic dispersions of colloidal rods. *Phys. Rev. E: Stat. Phys., Plasmas, Fluids, Relat. Interdiscip. Top.* **1998**, *58*, 7668−7677.
(31) Choi, I.; Smith, R. W. Kinetic study of dissolution of asbestos fibers in water. *J. Colloid Interface Sci.* **1972**, *40*, 253.
(32) Kuroda, A.; Nishimura, T.; Ishida, T.; Hirota, R.; Nomura, K. Detection of chrysotile asbestos by using a chrysotile-binding protein. *Biotechnol. Bioeng.* **2008**, *99*, 285−289.
(33) Phenrat, T.; Song, J. E.; Cisneros, C. M.; Schoenfelder, D. P.; Tilton, R. D.; Lowry, G. V. Estimating attachment of nano- and submicrometer-particles coated with organic macromolecules in porous media: Development of an empirical model. *Environ. Sci. Technol.* **2010**, *44*, 4531−4538.
(34) Mossman, B. T.; Bignon, J.; Corn, M.; Seaton, A.; Gee, J. B. L. Asbestos - scientific developments and implications for public-policy. *Science* **1990**, *247*, 294−301.
(35) Dresher, W. H.; Naumann, A. W. Chrysotile asbestos fiber dispersion including monocarboxylic acid. U.S. Patent 3,409,499 A, Nov 5, 1968.
(36) Crocker, J. C.; Grier, D. G. Methods of digital video microscopy for colloidal studies. *J. Colloid Interface Sci.* **1996**, *179*, 298−310.
(37) Broersma, S. Rotational diffusion constant of a cylindrical particle. *J. Chem. Phys.* **1960**, *32*, 1626−1631.
(38) Broersma, S. Viscous force and torque constants for a cylinder. *J. Chem. Phys.* **1981**, *74*, 6989−6990.
(39) Sokolov, I. M. Models of anomalous diffusion in crowded environments. *Soft Matter* **2012**, *8*, 9043−9052.
(40) Edwards, S.; Evans, K. Dynamics of highly entangled rod-like molecules. *J. Chem. Soc., Faraday Trans. 2* **1982**, *78*, 113−121.
(41) Michailidou, V.; Petekidis, G.; Swan, J.; Brady, J. Dynamics of concentrated hard-sphere colloids near a wall. *Phys. Rev. Lett.* **2009**, *102*, 068302.
(42) Helden, L.; Roth, R.; Koenderink, G. H.; Leiderer, P.; Bechinger, C. Direct measurement of entropic forces induced by rigid rods. *Phys. Rev. Lett.* **2003**, *90*, 048301.
(43) Haggerty, R.; Gorelick, S. M. Multiple-rate mass transfer for modeling diffusion and surface reactions in media with pore-scale heterogeneity. *Water Resour. Res.* **1995**, *31*, 2383−2400.
(44) Jackson, G. A.; Burd, A. B. Aggregation in the marine environment. *Environ. Sci. Technol.* **1998**, *32*, 2805−2814.
(45) Asgharian, B.; Yu, C. Deposition of inhaled fibrous particles in the human lung. *J. Aerosol Med.* **1988**, *1*, 37−50.
(46) Asgharian, B.; Yu, C.; Gradon, L. Diffusion of fibers in a tubular flow. *Aerosol Sci. Technol.* **1988**, *9*, 213−219.
(47) Gunes, D.; Scirocco, R.; Mewis, J.; Vermant, J. Flow-induced orientation of non-spherical particles: Effect of aspect ratio and medium rheology. *J. Non-Newtonian Fluid Mech.* **2008**, *155*, 39−50.
(48) Weitz, D.; Huang, J.; Lin, M.; Sung, J. Dynamics of diffusion-limited kinetic aggregation. *Phys. Rev. Lett.* **1984**, *53*, 1657.

DOI: 10.1021/acs.est.5b03839
Environ. Sci. Technol. 2015, 49, 13340−13349

(49) Ball, R.; Weitz, D.; Witten, T.; Leyvraz, F. Universal kinetics in reaction-limited aggregation. *Phys. Rev. Lett.* **1987**, *58*, 274.
(50) Lin, M.; Lindsay, H.; Weitz, D.; Klein, R.; Ball, R.; Meakin, P. Universal diffusion-limited colloid aggregation. *J. Phys.: Condens. Matter* **1990**, *2*, 3093.
(51) Ross, C. A.; Poirier, M. A. Protein aggregation and neurodegenerative disease. *Nat. Med.* **2004**, *10*, S10−S17.
(52) Hotze, E. M.; Phenrat, T.; Lowry, G. V. Nanoparticle aggregation: Challenges to understanding transport and reactivity in the environment. *J. Environ. Qual.* **2010**, *39*, 1909−1924.
(53) Keller, A. A.; Wang, H.; Zhou, D.; Lenihan, H. S.; Cherr, G.; Cardinale, B. J.; Miller, R.; Ji, Z. Stability and aggregation of metal oxide nanoparticles in natural aqueous matrices. *Environ. Sci. Technol.* **2010**, *44*, 1962−1967.
(54) Govers, G. Selectivity and transport capacity of thin flows in relation to rill erosion. *Catena* **1985**, *12*, 35−49.
(55) Sholl, D. S.; Skodje, R. T. Late-stage coarsening of adlayers by dynamic cluster coalescence. *Phys. A* **1996**, *231*, 631−647.

DOI: 10.1021/acs.est.5b03839
Environ. Sci. Technol. 2015, 49, 13340−13349